

Structural Performance of Concrete-Filled Tube Columns Using UHPC Compared to Conventional Concrete

Wanchai Yodsudjai¹, Nattapon Piyapong¹, Woradanai Wichitchaichakorn¹,
Supitchaya Sutthijessadaroj¹, Sitthinon Kaewsawang¹, Phattaraphong Ponsorn², Kirati Nitichote^{3,*}

¹Faculty of Engineering, Kasetsart University, Thailand

²Department of Civil Engineering, Faculty of Engineering, Rajamangala University of Technology Krungthep, Thailand

³Faculty of Science and Engineering, Kasetsart University Chalermphrakiat Sakon Nakhon Province Campus, Thailand

Received July 30, 2025; Revised December 30, 2025; Accepted January 20, 2026

Cite This Paper in the Following Citation Styles

(a): [1] Wanchai Yodsudjai, Nattapon Piyapong, Woradanai Wichitchaichakorn, Supitchaya Sutthijessadaroj, Sitthinon Kaewsawang, Phattaraphong Ponsorn, Kirati Nitichote, "Structural Performance of Concrete-Filled Tube Columns Using UHPC Compared to Conventional Concrete," *Civil Engineering and Architecture*, Vol. 14, No. 2, pp. 655 - 665, 2026. DOI: 10.13189/cea.2026.140201.

(b): Wanchai Yodsudjai, Nattapon Piyapong, Woradanai Wichitchaichakorn, Supitchaya Sutthijessadaroj, Sitthinon Kaewsawang, Phattaraphong Ponsorn, Kirati Nitichote (2026). *Structural Performance of Concrete-Filled Tube Columns Using UHPC Compared to Conventional Concrete*. *Civil Engineering and Architecture*, 14(2), 655 - 665. DOI: 10.13189/cea.2026.140201.

Copyright©2026 by authors, all rights reserved. Authors agree that this article remains permanently open access under the terms of the Creative Commons Attribution License 4.0 International License

Abstract The primary objective of this research is to compare the performance of columns filled with Ultra-High-Performance Concrete (UHPC) and those filled with normal concrete (NC) under controlled axial compressive forces. The experimental program was designed to fabricate specimens of both UHPC- and NC-filled tubes in the laboratory, ensuring consistency in size, steel tube thickness, and curing conditions. Each specimen was subjected to standardized axial loading tests to examine parameters, such as peak load capacity, deformation characteristics, and failure modes. The analytical part of the study focused on developing and validating models that accurately predict the structural response and ultimate strength of these composite columns. Special attention was paid to assessing the influences of steel tube wall thickness on the interaction between the steel and the concrete core, as well as the effectiveness of UHPC in enhancing strength and ductility. UHPC and NC-filled steel tube columns exhibited similar load-deformation behavior up to the maximum load. Nevertheless, UHPC showed a rapid drop in strength after the peak due to lower bonding and confinement effects. Both materials failed in similar modes, showing drum-shape deformation at the ends and shear failure in

the middle. Standard concrete-filled tube strength formulas were not reliable for UHPC, and increasing steel tube thickness was less effective for UHPC-filled columns than for those with normal concrete.

Keywords UHPC, Concrete-Filled-Tube, Failure Mode, FEM

1. Introduction

Currently, Concrete Filled Tube Columns (CFTs) are widely used structural elements in construction. CFTs are commonly used in the construction of high-rise buildings or large structures. Steel pipes resist axial force while enveloping concrete and concrete bears compression force while preventing buckling. The flexibility of steel tubes allows CFTs to achieve high strength and absorb energy before failure, making them suitable for earthquake resistance [1]. Thus, referring to Mosaberpanah and Eren [2], and Shanmugam and Lakshmi [3], steel pipes can replace wooden formwork, reducing construction time and construction costs. Ultra-high-Performance Concrete

(UHPC) has gained increasing popularity in construction thanks to its high strength, low porosity, and superior durability, which allow for reduced concrete volume and more complex architectural design. With the good properties of CFT and UHPC, they can be combined as a CFT column filled with UHPC, yielding a significantly higher efficiency [4]. However, in Thailand, there has been no research on UHPC-filled steel columns, as UHPC has not been widely used in the country [5]. It was also found that the main problem in the construction of CFT using UHPC is the rapid shrinkage of concrete, resulting in a lower efficiency of CFT due to the inability to transfer force [6]. With properties that obviously differ from normal concrete, the research on CFTs using normal concrete is therefore not referenceable. For these reasons, this study aims to investigate the behavior under compression of UHPC-filled steel tubes compared with NC-filled tubes, and to evaluate the performance of CFTs with different tube thicknesses.

Concrete-Filled Tube Columns (CFTs) have gained increasing attention in modern construction due to their exceptional structural performance and versatility. In these columns, a steel tube serves dual functions as formwork and a load-carrying member, while the concrete core provides compressive strength and prevents the steel tube from local buckling. This combination results in composite columns that are able to bear significant loads, resist seismic actions, and absorb energy efficiently, making them ideal for high-rise buildings, bridges, and structures in seismic zones.

A notable advancement in CFT technology is incorporating Ultra-High-Performance Concrete (UHPC) as the infill material. UHPC distinguishes itself from ordinary concrete with its ultrafine particle size, densely packed matrix, and the addition of fibers. These characteristics allow UHPC to achieve noticeably higher compressive strength than ordinary concrete, often exceeding 150 MPa, and to offer remarkable durability, reduced permeability, and increased resilience to environmental factors such as freeze-thaw cycles and chemical attacks. The use of UHPC in CFTs allows for the creation of slenderer, lighter columns without compromising load-bearing capacity or durability, thus supporting innovative architectural designs and reducing the overall quantity of materials needed.

In Thailand, however, the widespread application of such advanced materials and technologies is still limited. The primary challenges stem from factors such as the cost and availability of UHPC components, the need for specialized mixing and placing techniques, and a general lack of localized research data. For example, rapid shrinkage and associated cracking can occur in UHPC due to its low water-to-cement ratio, which may hinder proper bonding and stress transfer between the steel tube and the concrete core. This issue becomes particularly significant in the context of seismic performance, where composite

action is essential for energy dissipation and structural integrity.

Despite the global recognition of CFTs filled with UHPC, there remains a gap in research focused on their behavior under local conditions in Thailand—specifically, how variations in steel tube thickness and UHPC mix design affect the overall performance. Most studies to date have either concentrated on ordinary concrete or have relied on international data that may not account for regional material properties and construction practices. This lack of localized understanding can lead to conservative designs or missed opportunities for innovation in Thai infrastructure.

The motivation behind the present study is, therefore, to bridge this knowledge gap by systematically evaluating the structural behavior, failure mechanisms, and deformation patterns of CFTs filled with UHPC compared to those filled with normal concrete. Special attention is given to the influences of steel wall thickness on the axial load-bearing capacity and the nature of failure. By conducting controlled laboratory experiments and adhering to international testing standards, the research aims to provide engineers and designers with reliable data and practical guidelines for optimizing CFT columns in the Thai construction context. Ultimately, the goal is to promote the adoption of higher-performance, more efficient structural systems that satisfy both local and international safety and durability expectations.

2. Materials and Strength Evaluation Methods

The experimental program was designed to systematically evaluate the performance of both Ultra-high-performance concrete (UHPC) and normal concrete when used as an infill material inside circular steel tubes of varying wall thicknesses. Prior to casting, all steel tubes were thoroughly cleaned and measured to ensure dimensional accuracy and consistency among samples. After casting, the filled tubes were cured using the UltraMist system, curing using ultra-fine fog, for 28 days. Throughout the curing period, the specimens were monitored for early-age shrinkage and any visible defects.

Once the samples reached the specified testing age, axial compression tests were carried out to examine their load-bearing capacity and deformation characteristics. The setup included precise measurement devices to record displacement, strain distribution, and the ultimate failure mode of each specimen. All tests were conducted in accordance with relevant international standards to ensure the reliability and comparability of the results.

2.1. Normal Concrete (NC)

The normal concrete used in the experiment was mixed following the proportion given in **Table 1** and molded

into standard 200 mm-height and 100 mm-diameter cylindrical specimens. After the age of 28 days in moist curing, the compressive strength tests were eventually conducted according to ASTM C 39 standards. The tests were performed using a universal testing machine (UTM) with a capacity of 100 tons, applying a uniform rate of 1 mm/min. The compressive strength of the concrete was approximately 34.3 MPa.

Table 1. Mix proportion of NC

Cement (kg/m ³)	Water (kg/m ³)	Gravel (kg/m ³)	Sand (kg/m ³)	Water reducer (kg/m ³)
539	264	691	801	1.7

2.2. Ultra-High-Performance Concrete (UHPC)

This research work received support from Siam Cement Group Public Company Limited (SCG), the first company to invent the formula for special high-performance concrete in Thailand. The mix proportion is given in **Table 2**. To achieve the designed flow rate, a polycarboxylate-based superplasticizer was also added. After moist curing, at the age of 28 days, the specimens were subjected to the compression test in the same manner as the normal concrete specimens, resulting in an average compressive strength of 137.0 MPa

Table 2. Mix proportion of UHPC

Cement (kg/m ³)	Water (kg/m ³)	Silica fume (kg/m ³)	Sand (kg/m ³)	Water reducer (ml/m ³)	Micro Steel fiber (kg/m ³)
963	187	138	1,101	23,800	120

2.3. CFT Column Specimens

The twelve CFT specimens were divided into four batches, three specimens each, according to concrete types and tube wall thicknesses. They are summarized in **Table 3**. The specimens were produced by casting concrete into 76 mm-diameter and 250 mm-height steel pipes, as shown in **Figure 1**. After casting, clear plastic was used to cover the top end of the steel pipes, and the specimens were cured in the UltraMist curing room, where ultra-fine fog is employed to maintain proper humidity for concrete curing, for 28 days.

Table 3. Summary of specimens

Batch NO.	Concrete type	Tube thickness (mm)	No. of specimens	Notation
1	UHPC	3	3	U3
2	UHPC	2	3	U2
3	NC	3	3	N3
4	NC	2	3	N2



Figure 1. Casting the specimens

2.4. Testing

The compression tests for the ultimate compressive strength of the CFT specimens were conducted using a testing machine, ID CM 12, with a capacity of 300 tons. The strain was measured along the axis using one strain gauge installed at the midpoint of the steel pipe. Once the specimen was positioned in the testing machine, pre-loading was performed, and the weight was released to reduce the gap and friction between the loading plate and the test specimen, as well as to check the readiness of the equipment. The sample was then compressed by gradually increasing the load at a uniform rate of 2 kN per second, while collecting strain data from the strain gauge using a DCS 100A Data Logger until the column failed. However, the load was yet applied on the test column to confirm whether the specimen could still carry the load after the failure.

2.5. Strength of CFT Column

To estimate the compressive strength of CFT columns, the equation provided by the American Institute of Steel Construction (AISC) [7] can be employed. However, there is a limitation in concrete strength and a requirement for longitudinal rebars and lateral ties or spirals. An alternative method can be found in the study conducted by Yu et al. [4]. The study proposed the equation to evaluate the compressive strength of short CFT columns containing parameters representing concrete type and age. For CFTs using circular hollow steel sections at mature age, the compressive strength can be expressed as Eq.(1).

$$N_0 = \left(1 + \alpha \frac{\xi}{\xi + 1} \right) (A_c f_{ck} + A_s f_y) \quad (1)$$

where,

N_0 = Compressive strength (force) of CFT columns

A_c = Cross-sectional area of concrete

f_{ck} = Compressive strength of a cylindrical sample of concrete

A_s = Cross-sectional area of steel tube

f_y = Yielding strength of steel

α = Coefficient considering the interaction between concrete and steel tube

ξ = Confinement factor = $(A_s f_y) / (A_c f_{ck})$

The equation consists of two parts. The front part represents the effects of confinement. The coefficient considering the interaction between concrete and steel tube (α) depends on the mechanical properties of concrete. It was proposed in [4] that α can be set to be equal to 0.5 for normal concrete, while it is 0.3 for UHPC. The smaller value for UHPC denotes its higher modulus of elasticity and lower lateral deformation compared to normal concrete. The latter part denotes the total strength of a concrete core and steel wall.

3. Experimental Results

3.1. Load-Carrying Behavior

Load-carrying capacities of the CFT specimens obtained from the compression tests are summarized in **Table 4** and **Figure 2**. The NC- and UHPC-filled 3 mm wall thickness columns (denoted as N3 and U3 respectively) achieved the compressive strengths of 465.1 kN and 692.2 kN respectively. These capacities were higher than those using 2 mm wall thickness, which achieved 360.6 kN for the NC-filled specimen (N2) and 640.0 kN for the UHPC-filled specimen (U2).

All tested specimens exhibited similar behavior under the applied load as illustrated in **Figure 3**, showing load-displacement curves of the specimens. It needs to be noted that the graph of U2 could not be recorded after the peak load due to technical problems. The plots coincide with the specimens experiencing shear failure in the experiment conducted by Yu et al [4]. The plots consist of four regions. At the beginning, the specimens were in an elastic range where load and deformation were proportional. There was no clear deviation in the stiffness between the NC-filled and UHPC-filled specimens. When the applied load approached 80-90% of their ultimate load, the specimens were subjected to plastic deformation, causing a drum-shape deformation at the ends of the

specimens. The stiffness gradually declined until reaching the ultimate load.

After accomplishing the maximum load, the carried load descended due to shear failure in the middle of the specimens. Although all specimens experienced the shear failure, different manners were observed between the types of concrete. The UHPC-filled specimens tended to immediately decrease, while the NC-filled specimens tended to be more gradual. This was dedicated to the confinement factor (ξ), which also reflects the strength ratio of the steel wall to the concrete core. The UHPC-filled specimens had ξ that was far less than 1.0, meaning that the concrete core was noticeably stronger than the steel wall. When the core failed, the carried load was redistributed to the steel wall, while the load at this point exceeded the strength of the wall, resulting in an immediate drop of load. Contrastingly, the N2 had ξ that was near 1.0, and N3 had ξ that was higher than 1.0, respectively. This means that the concrete core and the steel wall had a similar strength for N2, and the core was weaker than the steel wall for N3. Hence, the wall still fairly carried the load, although the total strength was lost due to the core failure. Moreover, coarse aggregate in normal concrete delayed concrete deformation by mechanical interlocking, resulting in a gradual decrease. This behavior is not common in UHPC since it does not normally contain coarse aggregate. Nevertheless, all columns were still able to maintain a high level of load, although shear failure at the middle initiated.

After descending, the load was able to increase again. It was possible that the steel wall entered a strain-hardening region, causing higher stress to develop. For N3, this manner is possible to observe if the displacement increases further than the test limit, 25 mm. The typical load-displacement curve of CFT columns and the corresponding deformation are summarized in **Figure 4**.

The load-displacement plots inform us that CFT columns are ductile members. This could be attributed to the presence of the surrounding steel wall, which prevented free deformation of the cracked concrete core despite the initiation of shear failure. The applied force could yet be fairly, but not fully effective, transferred through the cracked concrete core and the deforming steel pipe.

Table 4. Ultimate compressive force of CFTs

Sample	Steel pipe		properties		Confinement factor, ξ	Ultimate compressive force (kN)
	D_{out} (mm)	D_{in} (mm)	f_y (MPa)	f'_c (MPa)		
U3	75.8	71.1	393.5	137.0	0.392	692.2
U2	75.9	72.7	362.6	137.0	0.239	640.0
N3	75.8	71.1	393.5	34.3	1.567	465.1
N2	75.9	72.7	362.6	34.3	0.953	360.6

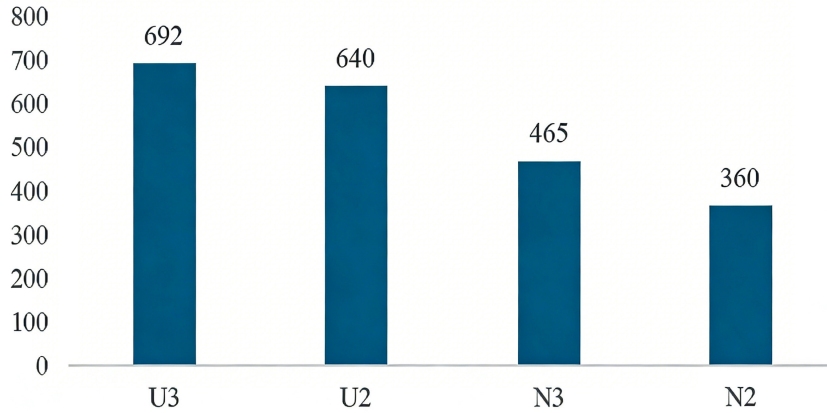


Figure 2. Ultimate compressive force of the CFT specimens

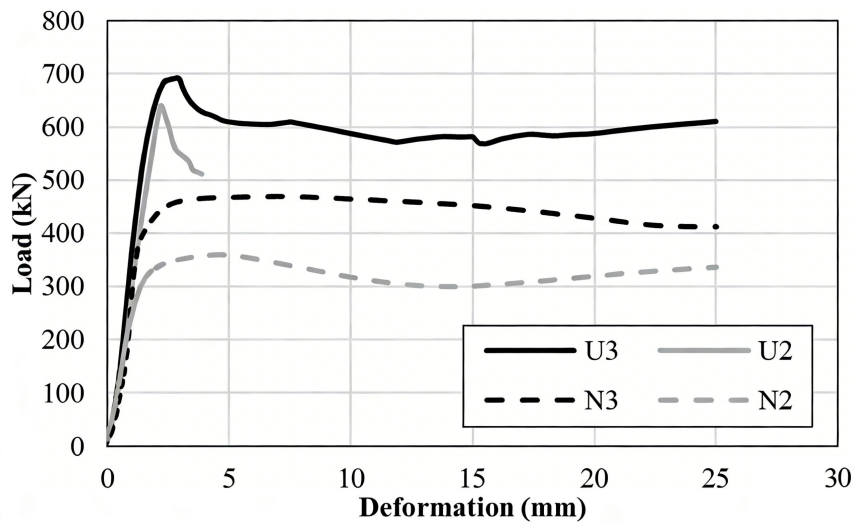


Figure 3. Load-displacement curves of the CFT specimens

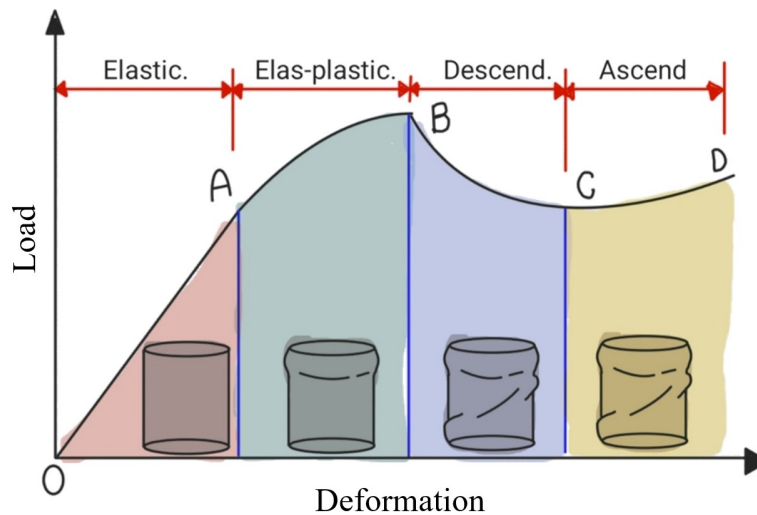


Figure 4. Typical load-displacement curve of CFT columns

3.2. Failure Mode

Figure 5 illustrates the two types of failures occurring in one specimen, and those are shear failure and drum-shape failure [8].

From the tests, it was found that all CFT specimens

exhibited similar failure modes, including the drum-shape upsetting failure and shear failure. At the ends, the drum-shape deformation occurred, while the parts of the specimens contacting the loading plates circularly bulged and laterally deformed. In the middle section, shear failure occurred, resulting in an inclined deformation.

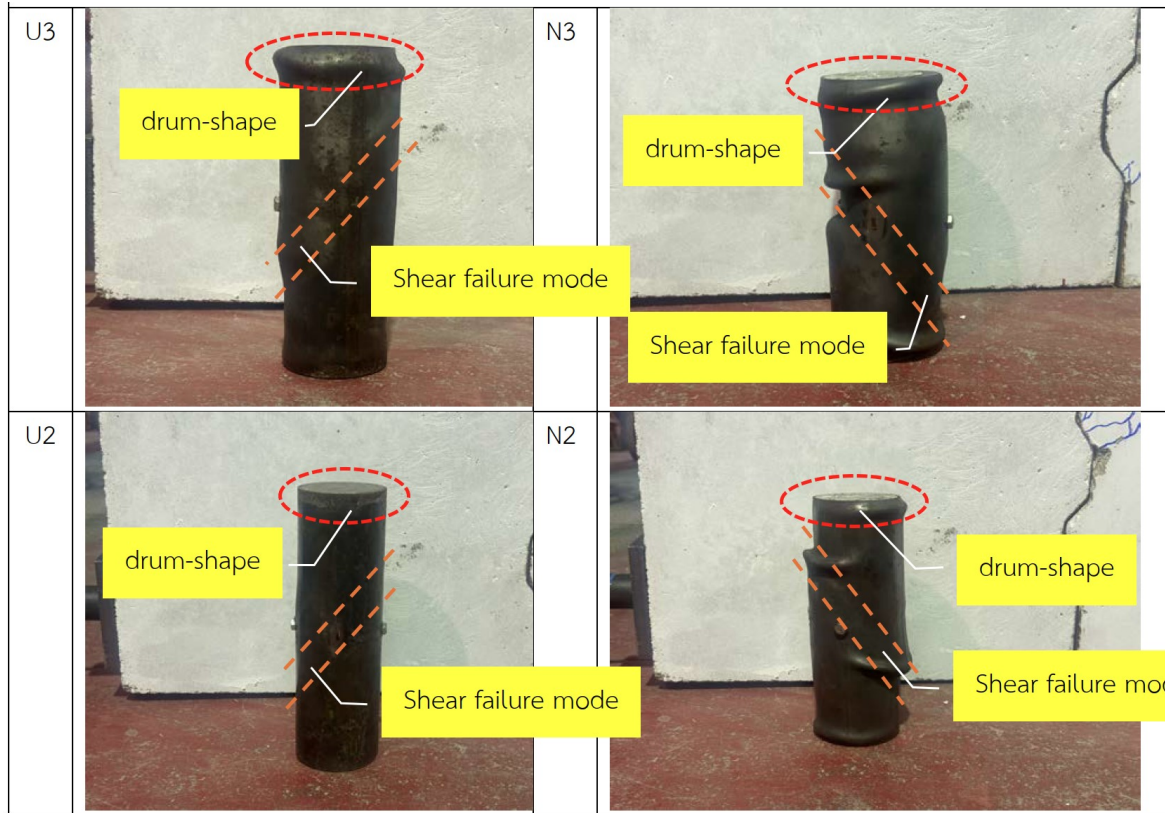


Figure 5. Failure mode of CFT

The drum-shape upsetting failure arose due to stress concentration under the loading plates. When compressive force is applied, stress is commonly intense at the load application point and gradually becomes uniform as a distance from the application point increases. The intense stress at the ends caused local buckling in steel and local cracks in concrete at the ends, appearing as the drum-shape upsetting failure [9]. Moreover, this deformation caused a load eccentricity which gradually reduced the ability to resist load and consequently affected shear deformation in the next stage. Nevertheless, the applied force could still be transferred.

Once the maximum load was reached, the shear failure appeared in the middle. The cracking sound was audible, and a minor steel deformation was visible when the failure started. Thus, it is possible that this failure was initiated by the failure of the concrete core and eventually deformed the steel wall. The compression failure of a concrete cylinder normally contains diagonal cracks. However, in the CFT specimens, the steel wall prevented a free deformation of the cracked concrete core. Therefore, instead of bursting, the cracked concrete diagonally pushed the steel wall and appeared as the diagonal shear failure at the middle section.

3.3. Comparison of Load-Bearing Capacities from Experiments and the Estimation

The load-bearing capacities obtained from the experiments (N_{test}) were compared to the values obtained

from an estimation using the equation from Yu et al. [4] (N_0) in this section. This is to examine the availability of the equation. The estimated results are numerically presented in **Table 5** and **Table 6** for the specimens with 2 and 3 mm-thick steel wall respectively, as well as being visualized in **Figure 6**. The results indicate accurate predictions for the NC-filled specimens, either with 2 or 3 mm-thick steel walls. The maximum error was 3.9% underestimated, which was a small error on the safe side. On the other hand, the estimation seems not to nicely work with the UHPC-filled specimens since it yielded the maximum 17.2% overestimation, which made the estimation on the unsafe side.

Table 5. Estimation results for the CFT specimens with 2 mm-thick steel wall

Concrete type	N_{test}	N_0	Error
	(kN)	(kN)	(%)
UHPC	640.0	736.0	+15.0
NC	360.6	346.7	-3.9

Table 6. Estimation results for the CFT specimens with 3 mm-thick steel wall

Concrete type	N_{test}	N_0	Error
	(kN)	(kN)	(%)
UHPC	692.2	811.4	+17.2
NC	465.1	456.4	-1.9

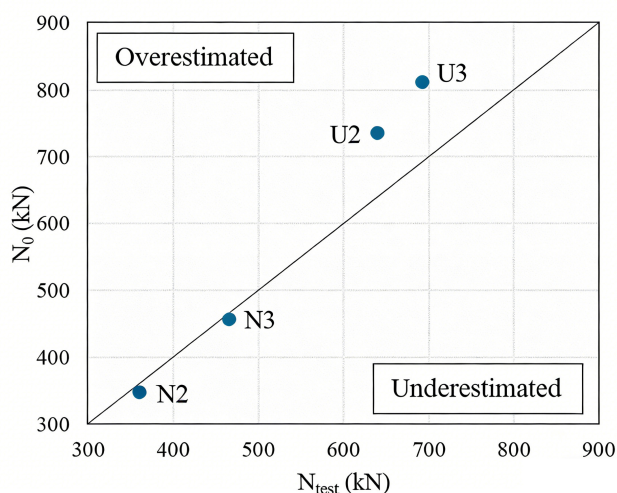


Figure 6. Comparison of load-bearing capacity from experiments and the estimation

However, the deviation in the estimation for UHPC-filled specimens is not harmonized with the Yu et al.'s [4] conclusion, which states that the equation provides a good estimation for either NC- or UHPC-filled columns. This could be attributed to several possible reasons. First, end stiffeners were installed on the specimens in [4] to prevent local failure due to stress concentration at the contacting areas. Only shear failure was thus observed. Contrastingly, there was no stiffener installed in the present study. The occurrence of the drum-shape failure may reduce the load-carrying capacity due to the resultant eccentricity. Moreover, high-strength concrete, such as UHPC, has a high possibility of strength variation, which possibly differs from the nominal value. Future research is recommended to focus on structural configurations and mechanical properties of UHPC that affect the performance of CFT columns to improve the applicability of the equation.

3.4. Effects of Wall Thickness of the Steel Pipes

The observations during testing revealed distinct behaviors between the specimens with different

thicknesses. The steel pipes exhibited noticeable deformation, particularly at points of potential weakness or imperfection along the cylinder. The column with a thinner wall, 2 mm, featured visible local buckling and early yielding, especially at the midsection where the strain gauge was attached and at the contact area with the loading plates. In contrast, the columns with 3 mm wall thickness exhibited higher resistance to deformation and a delayed onset of local buckling compared to those with 2 mm wall thickness. Therefore, the thicker steel wall improved the compressive strength of steel directly, as well as improving the confinement at a high level of load by delaying buckling, resulting in a strength increment.

Nevertheless, the strength increment was less effective in the UHPC-filled specimens than the NC-filled ones as presented in **Table 7**, informing the rise in compressive strength when thickening the steel wall from 2 to 3 mm, both obtained from the experiment and the equation. The table also informs us that the estimated increment (ΔN_0) is also able to reflect this phenomenon. However, the ΔN_0 for the UHPC-filled specimens significantly differed from the increment obtained from the tests (ΔN_{test}), 44.6%. This significant difference could be a result of the discrepancy in the estimation, which was mentioned in section 3.3.

The reasons for the lesser strength increment in the UHPC-filled specimens would be attributed to the confinement effect and composite action that require the interaction of the two materials. Basically, the concrete core laterally expands when it is axially compressed due to Poisson effect. Concurrently, the steel wall confines and prevents the core from being split due to the lateral deformation. This phenomenon also increases contact performance between the two materials, inducing them to effectively work as a composite section. Nonetheless, UHPC generally has a higher modulus of elasticity [9] and lower lateral expansion [10,11] than normal concrete. The smaller lateral expansion lowers the effectiveness of the confinement achieved by the steel wall. Even though using thicker walls, the performance might not effectively increase. In addition, the ability of the concrete core to prevent wall local buckling is also weakened. This could reduce the availability of the equation.

Table 7. Comparison of the increased ultimate force when increasing the thickness of the steel pipe

Concrete type	N_0	N_0	ΔN_0	N_{test}	N_{test}	ΔN_{test}	Diff. of ΔN_0 & ΔN_{test}
	2 mm	3 mm		2 mm	3 mm		
	(kN)	(kN)	(kN)	(kN)	(kN)	(kN)	(%)
UHPC	736.0	811.4	+75.4	640.0	692.2	+52.2	44.6
NC	346.7	456.4	+109.7	360.6	465.1	+104.5	4.9

4. Finite Element Analysis (FEA)

4.1. Concrete Model

In the finite element simulation, the concrete damage model employed was the Menetrey-Willam model, using the mechanical properties detailed in Table 8. The biaxial concrete compressive strength was calculated as Eq. (2). Poisson's ratio of 0.2, following ACI 318-25 [12], while the modulus of elasticity and concrete tensile strength were calculated using Eq. (3) and Eq. (4), respectively.

$$f'_{c,bi} = \left(1.2 - \frac{f'_c}{1000}\right) f'_c \quad (2)$$

$$E_c = 4700 \sqrt{f'_c} \quad (3)$$

$$f_t = 0.62 \sqrt{f'_c} \quad (4)$$

where,

$f'_{c,bi}$ = biaxial compressive strength (MPa)

f'_c = uniaxial compressive strength (MPa)

E_c = Modulus of elasticity (MPa)

f_t = Tensile strength

Table 8. Mechanical properties of concrete model

Type	E_c (MPa)	Poisson's ratio	f'_c (MPa)	f_t (MPa)	$f'_{c,bi}$ (MPa)
UHPC	55,012	0.2	137	7.23	145.63
NC	27,526	0.2	34.3	3.63	39.98

4.2. Steel Model

The steel properties were defined as a bilinear isotropic material with small hardening of the tangent modulus of 1450 MPa. The Young's modulus is 200 GPa, the yield strengths of nominal thicknesses 3 mm and 3 mm are 393.5 MPa and 362.6 MPa, respectively.

4.3. Element Configurations

The element type adopted in this analysis is SOLID186, having a higher-order 3D 20-node solid element that exhibits quadratic displacement behavior. The element is defined by 20 nodes having three degrees of freedom per node: translations in the nodal x, y, and z directions. The element supports plasticity, large deflection, and large strain capabilities. To a calibration element size, finite element convergence has been conducted in this study. A range of concrete element sizes from 40x40 mm down to a refined size of 5x5 mm was selected. Based on the convergence results presented in Figure 7, the concrete element size of 10x10 mm is deemed sufficient to be

adopted for this study since it provided the harmonized result with the experiment, and there was no improvement even though the size was smaller. For the steel tube element, a more refined size of 2x2 mm was adopted. It is noted that element sizes exceeding approximately 20 mm are too large and may be incompatible with the circular specimen dimensions for this study.

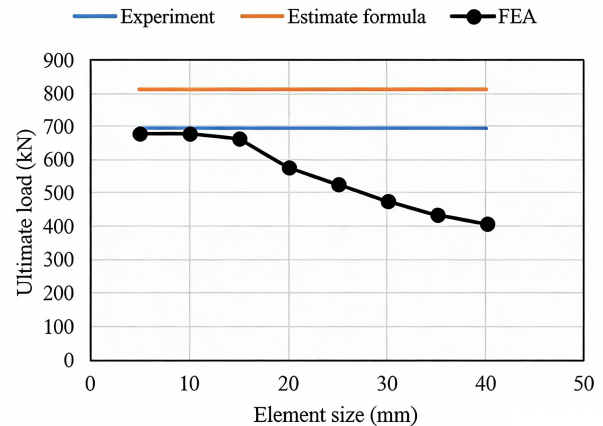


Figure 7. FE convergence results compared to example U3

4.4. Boundary Conditions

For finite element simulation, the top and bottom end supports were constrained as remote displacement, as shown in Figure 8. At both supports, the displacements and rotations in x, y, z are constrained to zero. The top support, where the load displacement is applied, is similar to the bottom one except that it permits the y displacement to enable the load-displacement control.

4.5. Simulation Results

4.5.1. Load-Carrying Capacity (N_{FEA})

The setting explained above yielded the results of the load-carrying capacity and the corresponding axial deformation presented in Table 9. Compared to the experimental results, it was found that the FEA gave precise results for load-carrying capacity prediction. The errors were in a small range either NC-filled or UHPC-filled specimens, in the range of 1.9% – 8.7% underestimation. This is different from the estimating equation, Eq. (1), as the comparison presented in Figure 9. It can be seen that the capacity obtained by the estimating equation only coincides when applying to the NC-filled columns, while the FEA results are harmonized when applying to both types. Therefore, it can be concluded that the model settings for FEA explained above are reasonable to be utilized simulations of both NC-filled and UHPC-filled columns. Nevertheless, the availability of the settings on other model configurations should be further investigated.

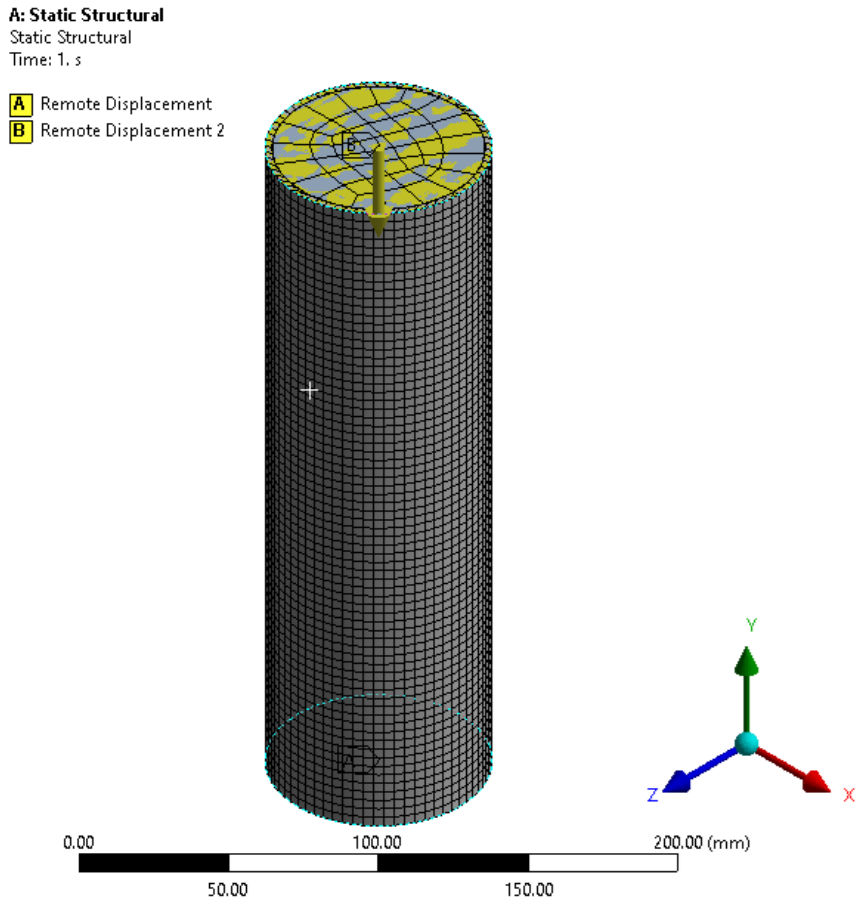


Figure 8. Boundary conditions for finite element simulation

Table 9. Results of finite element analysis

Model	N_{FEA} (kN)	Error from N_{test} (%)	Axial deformation at ultimate (mm)
U3	678.83	-1.9	-0.65
U2	602.71	-5.8	-0.61
N3	424.86	-8.7	-1.01
N2	348.7	-3.3	-1.05

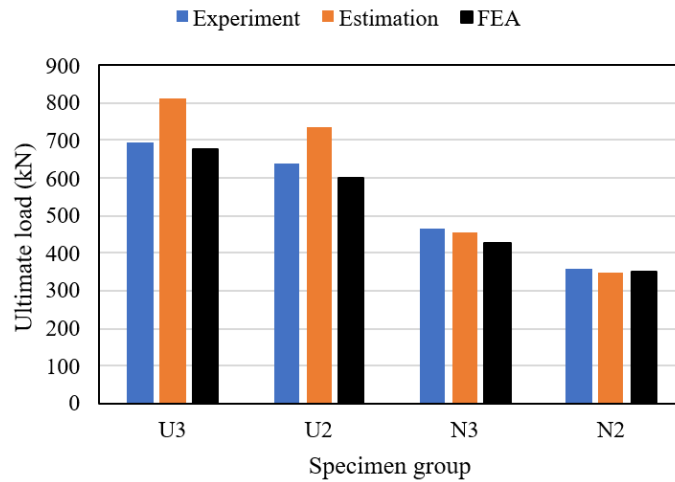


Figure 9. Comparison of ultimate compressive strength for CFT columns

4.5.2. Stress and Deformation

Stress and deformation captured from the simulation are illustrated in Figure 10. The colors denote the magnitudes of compressive stress. Blue color demonstrates high compressive stress, while a gradual transition to the warm tone colors shows the decrease in the stress, but still in compression.

The illustrations inform us that the compressive stress was intense at both ends, top and bottom, where contacting with the restraint points. These positions correspond with the drum-shape upsetting failure observed in the experiment. Hence, it supports the

explanation given in section 3.2 that the drum-shape deformation occurred due to stress concentration. It is suggested that CFT columns require end reinforcements, which can be either to the concrete core or the steel wall or both, to prevent the failure due to stress concentration.

Nevertheless, the shear failure could not be properly captured. The possible reason is that the shear failure occurred after the peak load, while the simulations targeted only the maximum load. Moreover, some simulation techniques might be required to properly visualize concrete failure.

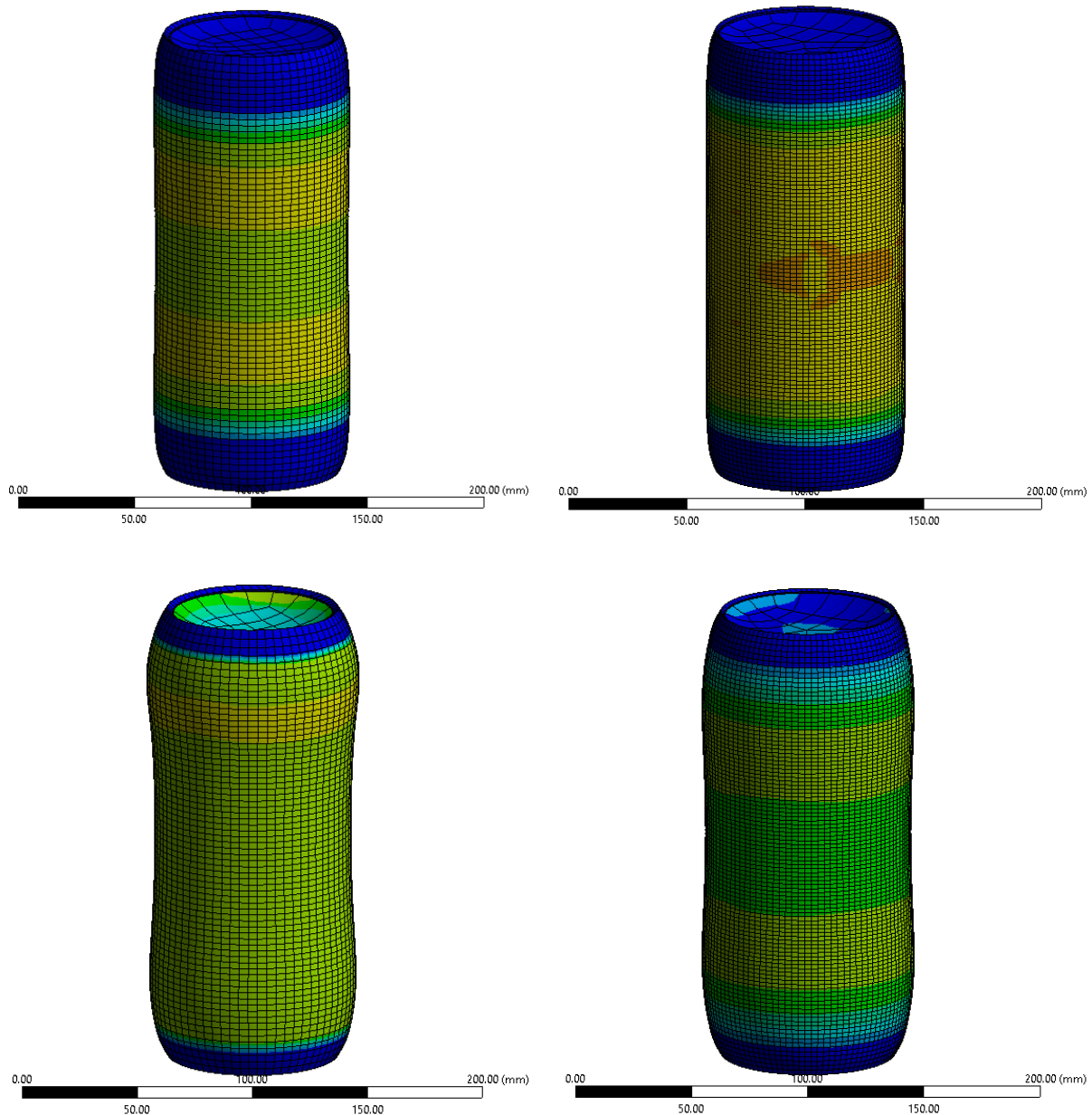


Figure 10. Results of finite element analysis for equivalent plastic strain at ultimate load (x5 deformation scale factor): (a) U3, (b) U2, (c) N3 and (d) N2

5. Summary

- a) NC-filled and UHPC-filled CFT columns exhibit similar load deformation curves. However, the UHPC-filled columns tend to immediately lose their strength after reaching the maximum load because the steel pipe is significantly weaker than the UHPC core. Contrastingly, the NC-filled columns tend to gradually lose their strength due to the comparable strengths of the two materials.
- b) The failure modes of CFTs, both NC and UHPC, have similar characteristics. A drum-shape upsetting failure at the ends of the columns, and a shear failure mode in the middle.
- c) The compressive strength predicting formula for CFTs is available for NC-filled columns, while some modifications are needed to predict the strength of UHPC-filled columns.
- d) High modulus of elasticity and low lateral expansion of UHPC decrease the confinement effect and composite action of CFT columns. Therefore, thickening the steel tube of UHPC-filled columns is less effective than that of NC-filled columns.
- e) Finite element analysis is able to precisely predict the load-carrying capacity of both NC-filled and UHPC-filled columns. Nevertheless, some additional modeling techniques might be needed to properly visualize the failures, and the availability of other model configurations should be further investigated.
- f) Reinforcements shall be provided at the end of CFT columns to prevent drum-shape upsetting failure due to stress concentration.

Acknowledgements

The authors would like to thank Kasetsart University for providing support, facilities, and testing equipment. The materials used in this test for producing UHPC were kindly offered by Saim Cement Group.

REFERENCES

- [1] Chiming C., Rui Z., Jia L.J., Yan W., "Structural behavior of UHPC filled steel tube columns under axial loading", *Thin-Walled Structures*, vol. 130, no. 5, pp. 550–563, 2018. DOI: 10.1016/j.tws.2018.06.016.
- [2] Mohammad A. M., Ozgur E., "Relationship between 28 days compressive strength and compression toughness factor of ultra-high performance concrete using design of experiments", *Procedia Engineering*, vol.145, pp. 1565–1571, 2016. DOI: 10.1016/j.proeng.2016.04.197.
- [3] Shanmugam N., Lakshmi B., "State of the art report on steel-concrete composite columns", *Journal of Constructional Steel Research*, vol. 57, no. 10, pp. 1041–1080, 2001. DOI: 10.1016/S0143-974X(01)00021-9.
- [4] Stephen S., Schneider, "Axially loaded concrete-filled steel tubes", *ASCE Journal of Structural Engineering*, vol. 124, no.10, pp. 1125–1138, 1998. DOI: 10.1061/(ASCE)0733-9445(1998)124:10(1125).
- [5] Krongchaiyong P., Pothasari W., Greerapla V., "The effect of lateral confinement on the ductility of square cross-section concrete-filled steel columns", in *The 25th National Civil Engineering Conference*, Burapha University, pp. 1–8, 2020. DOI: 10.1007/978-981-15-8079-6_164.
- [6] Shi C., Wu V., Xiao J., Wang D., "A review on ultra-high-performance concrete: Part I. Raw materials and mixture design", *Construction and Building Materials*, vol. 101, pp. 741–751, 2015. DOI: 10.1016/j.conbuildmat.2015.10.088.
- [7] American Institute of Steel Construction, "Specification for structural steel buildings", ANSI/AISC 360-22, American Institute of Steel Construction, Chicago, Illinois, 2022.
- [8] Chen M., Hou X., "Comparative Study on the Axial Compression and Bearing Capacity of Reactive Powder Concrete-Filled Circular Steel Tube", *Advances in Materials Science and Engineering*, vol. 2018, pp. 1–11, 2018. DOI: 10.1155/2018/8038649.
- [9] Han L., Li H., Bjorhovde R., "Developments and advanced applications of concrete-filled steel tubular (CFST) structures: Members", *Journal of Constructional Steel Research*, vol. 100, pp. 211–228, 2018. DOI: 10.1016/j.jcsr.2014.04.016.
- [10] Elremaily A., Azizinamini A., "Behavior and strength of circular concrete-filled tube columns", *Journal of Constructional Steel Research*, vol. 58, no. 12, pp. 1567–1591, 2002. DOI: 10.1016/S0143-974X(02)00005-6.
- [11] Sakino K., Nakahara H., Morino S., Nishiyama I., "Behavior of centrally loaded concrete-filled steel-tube short columns", *ASCE Journal of Structural Engineering*, vol. 130, no. 2, pp. 180–188, 2004. DOI: 10.1061/(ASCE)0733-9445(2004)130:2(180).
- [12] ACI committee 318, "Building Code for Structural Concrete. Code Requirements and Commentary (ACI CODE-318-25)", American Concrete Institute, Farmington Hills, Michigan, 2025.